# Towards a unified understanding: the linkage of MaxEnt, ETRHEQ, and SFE Models in estimating evapotranspiration

Yi Wang[1]*, Richard. M. Petrone[1], Mazda Kompanizare[1,2]

[1]Hydrometeorology Research Group, University of Waterloo, Waterloo, Ontario, Canada, N2L 3G1

[2]Global Institute in Water Security, University of Saskatchewan, 11 Innovation Blvd, Saskatoon, SK S7N 3H5, Canada

Corresponding author: yi.wang1@uwaterloo.ca

**Key Points:**

- The study presented a pure theorical analysis to unifying the MaxEnt, ETRHEQ and SFE within the same hydrometeorological framework
- Minimizing the dissipation function of energy fluxes in MaxEnt is equivalent to minimizing the vertical variance of RH in ETRHEQ
- The connection between MaxEnt, ETRHEQ, and SFE is independent of Monin-Obukhov similarity theory (MOST)'s extremum solution

**Abstract**: The maximum information entropy production model (MaxEnt), the relative humidity at equilibrium approach (ETRHEQ), and the Surface Flux Equilibrium model (SFE) are the three effective parsimonious models to estimate evapotranspiration. No attempts have been made to investigate their congruence, distinctions, or potential complementarity. Our mathematical analysis demonstrates that minimizing the dissipation function of energy fluxes in MaxEnt is equivalent to minimizing the vertical variance of RH in ETRHEQ. The effectiveness of both MaxEnt and ETRHEQ lies in the fact that far-from-equilibrium ecosystems progress toward a steady state (the SFE state) by minimizing dissipation. This tendency is manifested through the vertical variance of RH. The connection between MaxEnt, ETRHEQ, and SFE is independent of Monin-Obukhov similarity theory (MOST)'s extremum solution, and MOST's extreme solution can be viewed as equivalent to introducing a constant correction factor to account for atmospheric stability. While MaxEnt and ETRHEQ share a common physical foundation, they diverge in their approaches to modeling evapotranspiration, particularly in how they address the roles of vegetation and land surface heterogeneity. More importantly, the unified hydrometeorological framework suggests that turbulence fluxes within the atmospheric boundary layer adhere to the principles of maximum information entropy production. The way in which dissipation, along with its associated entropy production, is established using information entropy theory deviates from traditional thermodynamic entropy formulations. Delving into the precise computation of dissipation and entropy production for energy fluxes at different temporal and spatial scales presents an appealing avenue for prospective research.

**Plain Language Summary:** This paper seeks to establish a common physical basis for explaining the effectiveness of the maximum information entropy production model (MaxEnt), the relative humidity at equilibrium approach (ETRHEQ), and the Surface Flux Equilibrium model (SFE) in estimating evapotranspiration over a wide range of conditions. It uncovers that MaxEnt's approach to minimizing dissipation is equivalent to ETRHEQ's method of reducing the

vertical variance in relative humidity. Both models describe how ecosystems evolve towards a steady state (the basis of the SFE model) through minimizing dissipation, which is essentially equivalent to maximizing information entropy production. The paper suggests that the movement of air and energy in the lower atmosphere follows the principles of maximum information entropy production, a concept that is a bit different from traditional ideas of entropy in thermodynamics. This could lead to new insights in atmospheric science and land-atmosphere interactions.

**Keywords**: Maximum entropy, information entropy, the relative humidity at equilibrium, Surface Flux Equilibrium, theorical analysis

## 1. Introduction

The Earth's energy balance components, including terrestrial net radiation (Rn), and its partitioning into ground (G), sensible (H) and latent (LE) heat fluxes, impacts the global climate system and hydrological cycle (Dickinson, 1983; Duveiller et al., 2018). Among various energy components, LE, or its hydrologic equivalent, evapotranspiration (ET) links the energy and water balances and has attracted enormous research interest. Many models that estimate ET (e.g., Penman-Monteith and Priestley-Taylor equations) have been developed and widely used in various types of ecosystems (Monteith, 1965; Priestley and Taylor, 1972). The models generally require parameterizations of both land surface and atmospheric conditions, which are sometimes difficult to acquire. As a result, accurately modelling ET remains challenging.

Recently, emerging evidence suggests that atmospheric observations alone sometimes can be sufficient to estimate ET, and a novel, data-driven method (i.e., the relative humidity at equilibrium (ETRHEQ)) has thus been developed (Rigden and Salvucci, 2015; Salvucci and Gentine, 2013). ETRHEQ states that there is a trend towards minimizing the vertical variance in the relative humidity (RH) profile within the surface boundary layer throughout the day, which signifies a move towards thermodynamic equilibration between the land surface and the boundary layer (Salvucci and Gentine, 2013). Consequently, daily surface conductance ($C_{surf}$) is determined through an emergent relation between the diurnal cycle of the RH profile and ET. This relation reveals that the optimal daily $C_{surf}$, which yields the most accurate ET predictions, simultaneously minimizes the vertical variance of RH averaged over the course of the day (Rigden and Salvucci, 2015; Salvucci and Gentine, 2013). In the steady state, ETRHEQ can be explained by the Surface Flux Equilibrium (SFE) when humidity and heating terms in the RH budget are equivalent (McColl et al., 2019). In such state, the evaporation fraction (EF) can be simplified into a function of RH (Eq. 1) (McColl et al., 2019). This formula is also applicable for estimating LE, therefore, we refer to it as the SFE model, as described in Chen et al. (2021).

$$\mathrm{EF} = \frac{\mathrm{LE}}{\mathrm{R_n - G}} = \frac{\mathrm{LE}}{\mathrm{LE + H}} = \frac{\mathrm{RH}\varepsilon}{\mathrm{RH}\varepsilon + 1} \tag{1}$$

where RH is the atmospheric relative humidity, $\varepsilon = \delta \frac{\lambda}{c_p}$, $\delta$ is the slope of the relation between saturation vapor pressure and temperature, $\lambda$ is the latent heat of vaporization of water, $c_p$ is the specific heat capacity of air.

Another advanced approach to predict ET is based on the maximum information entropy production principle (MaxEnt) (Wang and Bras, 2009; Wang and Bras, 2011). MaxEnt is primarily concerned with probability distributions and seeks to find the probability distribution that maximizes the information entropy while satisfying certain constraints (Jaynes, 1957). While it is based on nonequilibrium statistical mechanics, research have revealed that MaxEnt does not contradict classical thermodynamic entropy within the framework of the maximum entropy production theory (MEP) (Dewar, 2005; Kleidon, 2009; Lent, 2019). The MEP theory states that the far-from-equilibrium ecosystems evolve with time to the steady state by maximize entropy production, or equivalently, by minimizing the dissipation (Prigogine and Lefever, 1973; Schneider and Kay, 1994). The dissipation represents the transformation of more complex energy forms into heat and the subsequent dispersion of this heat into the environment (Kleidon, 2009). The MaxEnt formulism for the entropy production of macroscopic fluxes was described by Dewar (2005). It was later incorporated into a predictive tool in modelling the energy and water fluxes of ecosystems by Wang and Bras, 2009, 2011. In this paper, we labeled Wang and Bra's model as the MaxEnt model to make a clear distinction from most recently SFE-MEP model that integrates SFE with the entropy production associated with the sensible heat (Kim et al., 2023). In the MaxEnt model, the dissipation (D) is formulized with energy fluxes and their corresponding thermal inertia parameters ($I_s$, $I_a$ and $I_e$), as (Wang and Bras, 2011) :

$$D(LE, H, G) = \frac{2G^2}{I_s} + \frac{2H^2}{I_a} + \frac{2LE^2}{I_e} \quad (2)$$

Hence, G,H and LE in MaxEnt is derived from the unique solution obtained by extremization of D under the energy balance constraint (Wang and Bras, 2011) as well as the extremum hypothesis of turbulent transport in the boundary layer with Monin-Obukhov similarity theory (MOST) (Wang and Bras, 2010).

The MaxEnt model, the SFE model and the ETRHEQ approach aim at providing the best estimates of ET based on limited site information. For MaxEnt, such information are net radiation, surface temperature and surface humidity (Wang and Bras, 2011), while for SFE, they are net radiation, air temperature and air humidity (Chen et al., 2021; McColl et al., 2019). The SFE and MaxEnt are both designed for use on temporal scales of a daily or larger extent. As for ETRHEQ, the required inputs are sub-daily meteorological variables including air temperature, air specific humidity, wind speed, air pressure, friction velocity, downwelling and upwelling shortwave/longwave radiation, and precipitation. The three approaches have demonstrated their applicability across a wide range of sites from arid to humid conditions (Chen et al., 2021; Salvucci and Gentine, 2013; Wang and Bras, 2011). Specifically, the MaxEnt model demonstrated superior performance on densely vegetated surfaces, such as tropical rainforests and well-watered wetland areas; and in contrast, it exhibits more pronounced deviations when applied to surfaces with shorter vegetation (e.g., shrublands) (Yang et al., 2022). The SFE model and the ETRHEQ model were applicable over inland continental regions, but were not suitable for sites with strong horizontal advection of moisture (e.g., coastal regions) and extremely dry or wet soil conditions (Chen et al., 2021; Raghav and Kumar, 2021).

While the ETRHEQ model has a physical basis explained within the framework of SFE, MaxEnt, despite its empirical success, lacks a corresponding hydrometeorological foundation. The three models all pertain to a state of "equilibrium", albeit with distinct definitions and formulation. Specifically, MaxEnt posits that ecosystems minimize the dissipation function toward equilibrium, whereas ETRHEQ asserts that ecosystems minimize the vertical variance of RH toward equilibrium. Both models illustrate the likeliest routes that ecosystems take to progress towards a state of equilibrium, or more succinctly, the steady state, and the SFE model represents the steady state. Their formulations that are based on Monin-Obukhov similarity theory (MOST) suggests a linkage between them. However, no attempts have been made to investigate their congruence, distinctions, or potential complementarity. While such understanding can greatly enhance our understanding on earth system thermodynamics and improve the development of hydrological models.

In this manuscript, we delve into the formulation of MaxEnt, ETRHEQ and SFE to explore their connections, initially examining the steady-state condition where environmental variables remain constant over time, and subsequently transitioning to non-steady-state conditions. Additionally, MaxEnt relies on a special formulation of the extremum solution of MOST, so we delve into the hydrometeorological basis of such extremum solution in MaxEnt, considering it as a unique case. Lastly, we address the limitations inherent in these models and deliberate upon their implications.

## 2. The connection between the MaxEnt, ETRHEQ, and SFE in the steady state

### 2.1 Under zero vertical gradient in relative humidity ($\frac{\partial \mathrm{RH}}{\partial \mathrm{z}} = 0$)

As explained in McColl et al. (2019), the steady state ETRHEQ satisfies the condition:

$$\left.\frac{\partial[(\mathrm{RH_s}(\mathrm{g_s}) - \mathrm{RH})^2]}{\partial \mathrm{g_s}}\right|_{\mathrm{g_s} = \mathrm{C_{surf}}} = 0 \qquad (3)$$

where RHs is the surface relative humidity ($\mathrm{RH_s} = \frac{\mathrm{q_s}}{\mathrm{q^*_{(T_s)}}}$) with $q_s$ the surface specific humidity and $q^*(T_s)$ the saturated surface specific humidity at surface temperature $T_s$; RH is the air relative humidity ($\mathrm{RH} = \frac{\mathrm{q}}{\mathrm{q^*(T)}}$) with q the air specific humidity, and $q^*(T)$ the saturated specific humidity at air temperature T; $g_s$ is the surface conductance, and $C_{surf}$ is the optimal surface conductance that minimizes the vertical variance of RH profile.

Such expression can be simplified into a closed-form expression for EF as Eq. 1. The details of the derivation of steady-state ETRHEQ solution are demonstrated in McColl et al. (2019).

In MaxEnt, the energy fluxes H and LE can be expressed using the profile of potential temperature (T) and surface specific humidity ($q_s$) (Wang and Bras, 2009; Wang and Bras, 2011), as:

$$H = -\rho c_p K_H \frac{\partial T}{\partial z} \tag{4}$$

$$LE = -\lambda \rho K_H \frac{\partial q_s}{\partial z} \tag{5}$$

With the eddy-diffusivity $K_H$ being determined based on the extremum solution of the Monin-Obukhov similarity theory (MOST) and Businger et al. (1971)'s flux-profile relationship, as (Wang and Bras, 2009):

$$K_H = C_1 \kappa z u^* \tag{6}$$

where $\rho$ is the density of air, $c_p$ is the specific heat capacity of air, $\lambda$ is the latent heat of vaporization of water, $\kappa$ is the von Karman constant, z is the distance above the evaporative surface, u* is the friction velocity, and $C_1$ is the coefficient related to the stability of the mean profile of the wind speed and the potential temperature, with $C_1$ being $\frac{\sqrt{3}}{\alpha}$ and $\frac{2}{1+2\alpha}$ under unstable and stable atmospheric condition, respectively, and $\alpha$ is a constant taken as 0.75 or 1 (Wang and Bras, 2009).

The vertical profile of RH can be determined through the chain rule as (detailed derivation in Appendix A):

$$\frac{\partial RH}{\partial z} = \frac{1}{q^*(T)} \left(-\delta \cdot RH \cdot \frac{\partial T}{\partial z} + \frac{\partial q}{\partial z}\right) \tag{7}$$

where $\mathrm{RH} = \frac{q}{q^*(T)}$, q*(T) is the saturated specific humidity at temperature T, and $\delta = \frac{\partial q^*(T)}{\partial T}$.

In idealized condition, the air in the boundary layer is well mixed, suggesting that the vertical gradient of relative humidity is zero. This assumption is the same as the assumption for the box model in McColl et al. (2019), where the box was assumed to be well mixed, implying zero vertical gradients of potential temperature and specific humidity. By letting $\frac{\partial \mathrm{RH}}{\partial z} = 0$, we get the following from Eq.7:

$$\frac{\partial q}{\partial z} = \delta \cdot \mathrm{RH} \cdot \frac{\partial T}{\partial z} \tag{8}$$

Wang and Bras (2011) pointed out that employing specific humidity at some finite distance above the surface remains valid and $q \approx q_s$. Furthermore, by substituting '$q_s$' with 'q' and assuming that the stability of the mean temperature and water vapor profiles is the same, Equations 4 and 5 yield expressions identical to MOST's fluxes expressions. This assumption of same stability of mean temperature and water vapor profiles has been widely used in evapotranspiration models including ETRHEQ.

Combining this with Eq 4, 5 and 8, the evaporative fraction (EF) can be rearranged as:

$$\mathrm{EF} = \frac{\mathrm{LE}}{\mathrm{LE}+\mathrm{H}} = \frac{1}{1+\frac{\mathrm{H}}{\mathrm{LE}}} = \frac{1}{1+\frac{c_p}{\lambda\delta\mathrm{RH}}} = \frac{\mathrm{RH}\varepsilon}{\mathrm{RH}\varepsilon+1} \tag{9}$$

with $\varepsilon = \delta\frac{\lambda}{c_p}$.

Eq. 9 that is derived from MaxEnt is exactly equivalent to Eq. 1, showing that MaxEnt is consistent with ETRHEQ and SFE in the steady state when vertical gradient of RH is zero.

## 2.2 Under non-zero vertical gradient in relative humidity ($\frac{\partial \mathrm{RH}}{\partial z} \neq 0$)

In order to investigate the connection between the dissipation function in MaxEnt and the vertical profile of RH, we incorporated a rearranged RH-based Penman–Monteith (PM) equation (the $PM_{RH}$ model) provided by Kim et al. (2021). The $PM_{RH}$ model aligns with the classical PM equation which is derived from principles of energy balance and mass transfer theory. The $PM_{RH}$ model presents these concepts by expressing them in terms of RH and $RH_s$, facilitating a more straightforward rearrangement of the dissipation function expressed by RH gradients. The $PM_{RH}$ model is expressed as (Kim et al., 2021):

$$LE = \frac{RH_s \delta (Rn - G)}{RH_s \delta + \gamma} + \frac{\rho c_p q^*\left(T_s\right)\left(RH_s - RH\right) g_a}{RH_s \delta + \gamma} \tag{10}$$

The sensible heat flux (H) is expressed as (McColl et al., 2019):

$$H = \rho c_p g_a (T_s - T) \tag{11}$$

with linearizing the relationship between saturated specific humidity and temperature:

$$q^*(T_s) = q^*(T) + \delta(T_s - T) \tag{12}$$

where $g_a$ is the aerodynamic resistance, and $\gamma = \frac{c_p}{\lambda}$.

As stated, the dissipation (D) is formulized with energy fluxes and their corresponding thermal inertia parameters ($I_s$, $I_a$ and $I_e$) (Wang and Bras, 2011; Yang et al., 2022), and the three inertia parameters are defined as:

$$I_s = \sqrt{I_d^2 + \theta\, I_w^2} \tag{13}$$

$$I_a = \rho c_p \sqrt{K_H} \tag{14}$$

$$I_e = \sigma I_a \tag{15}$$

where $I_d$ is the thermal inertia of dry soil and set as 800 tiu for the representative value, θ is the volumetric soil soisture, $I_w$ is the thermal inertia of still liquid water and set as 1557 tiu, and σ is a parameter characterizing the change of near surface specific humidity ($q_s$) with changes of near surface temperature ($T_s$).

Based on Eq. 4, 11 and 14, the eddy diffusivity ($K_H$) and aerodynamic conductance ($g_a$) are linked through the understanding that higher eddy diffusivity (implying more efficient turbulent mixing) corresponds to lower resistance to scalar transfer, and vice versa, and therefore, $K_H = g_a$. It is noted that such a relationship is more of a conceptual understanding derived from the basic principles of turbulent transfer in the atmospheric surface layer, as explained in Stull (1988). As a result, $I_a$ can be expressed as:

$$I_a \equiv \rho c_p \sqrt{g_a} \tag{16}$$

Under the constraint of energy closure, substituting Eq. 10, 11, 15, 16 leads to a quadratic expression as (detailed derivation in Appendix B):

$$\begin{aligned} & D = a\left(-RH_s + RH\right)^2 + b\left(-RH_s + RH\right) + c, \\ & \text{with} \quad a = \frac{2q^*\left(T_s\right)^2 c_p g_a^{\,2}(\sigma + 1)\,\rho}{\sqrt{g_a}\left(RH_s\delta + \gamma\right)^2 \sigma}, \\ & b = -\frac{4q^*\left(T_s\right) c_p g_a\left(-RH_s\delta + \gamma\sigma\right)(-Rn + G)\,\rho}{\sqrt{g_a}\left(RH_s\delta + \gamma\right)^2 \rho c_p \sigma}, \\ & c = \frac{2I_s(-Rn + G)^2\left(RH_s^{\,2}\delta^2 + \gamma^2\sigma\right) + 2G^2\left(RH_s\delta + \gamma\right)^2 \rho c_p \sqrt{g_a}\,\sigma}{\sqrt{g_a}\,I_s\left(RH_s\delta + \gamma\right)^2 \rho c_p \sigma}. \end{aligned} \tag{17}$$

For given Rn, $q_s$, $T_s$ and $g_a$ in an ecosystem, D can be expressed as a quadratic function with regards to RH-$RH_s$ (Eq. 17). The minimum value of the quadratic equation D occurs at X, with

$$X = \frac{-RH_s \delta G + G\gamma\sigma + RH_s \delta Rn - Rn\gamma\sigma}{q^*\left(T_s\right) c_p g_a \rho(\sigma + 1)} \tag{18}$$

In order to determine X, we first formulate σ. Recall that $\sigma = \frac{\lambda}{c_p}\frac{\partial q_s}{\partial T_s}$ in MaxEnt. Wang and Bras (2011) implemented Edlefsen and Anderson (1943)'s model that related surface specific humidity ($q_s$) to surface temperature ($T_s$), as:

$$q_s = \epsilon \frac{e_0}{P_0} \exp[\frac{\lambda}{R_v}\left(\frac{1}{T_0} - \frac{1}{T_s}\right)] \exp(-\frac{g\psi_s}{R_v T_s}) \tag{19}$$

Hence, the expression written in terms of σ can be simplified into (Wang and Bras, 2011):

$$\sigma = \frac{\lambda}{c_p}\frac{\partial q_s}{\partial T_s} = \frac{\lambda^2 q_s}{c_p R_v T_s^2}(1 + \frac{g\psi_s}{\lambda}) \cong \frac{\lambda^2 q_s}{c_p R_v T_s^2} \tag{20}$$

where ϵ is the dimensionless ratio of the gas constant for dry air to water vapor (0.622), $T_0$ is the reference temperature (0 °C), $e_0$ is the saturated vapor pressure at $T_0$, $P_0$ is the ambient pressure, $R_v$ is the gas constant for water vapor, $\psi_s$ is the soil water potential, and g is the acceleration of gravity.

Wang and Bras (2011) pointed out that the formula of σ (Eq. 20) they provided was a postulation. Instead, we use the chain rule to derive the expression for σ, as:

$$\sigma = \frac{\lambda}{c_p}\frac{\partial q_s}{\partial T_s} = \frac{\lambda}{c_p}\frac{\partial q_s}{\partial q^*(T_s)}\frac{\partial q^*(T_s)}{\partial T_s} = \frac{\delta\lambda}{c_p}\frac{\partial q_s}{\partial q^*(T_s)} = \frac{\delta}{\gamma} RH_s \tag{21}$$

Given $q_s = RH_s \cdot q^*(T_s)$.

The postulation from Eq. 21 aligns with the Clausius-Clapeyron equation for determining $q_s$ from $RH_s$ and $T_s$. This approach is utilized by ETRHEQ (Rigden and Salvucci, 2015) as well as by MaxEnt in the condition where the soil water retention curve is unknown (Wang and Bras, 2009). Additionally, the validity of Eq. 21 is supported by examining the extreme cases of completely dry and fully saturated surfaces. As explained in Wang and Bras (2009) when the surface is completely dry, $\sigma = 0$ as RHs = 0; while in a saturated state, $\sigma = \frac{\delta}{\gamma}$ as $RH_s$ =1.

Substituting Eq 21. into Eq. 18,

$$X \equiv 0$$

Therefore, the minimum value of the quadratic equation D occurs at $RH_s$=RH. The dissipation D decreases as the absolute difference between $RH_s$ and RH (e.g., $|RH-RH_s|$) decreases, and vice versa.

Clearly, minimizing dissipation function of the energy fluxes in MaxEnt is equivalent to minimizing the vertical difference of RH. When using two levels, minimizing the vertical difference of RH is equivalent to minimizing the vertical variance of RH in ETRHEQ, and the vertical variance of RH is affected by the surface conductance (which is presented in Section 3). The empirical success of both MaxEnt and ETRHEQ lies in the fact that the far-from-equilibrium ecosystems move towards the steady state by maximizing the production of information entropy and minimizing dissipation. This tendency is manifested through the vertical difference of RH. When these ecosystems reach the idealized condition (i.e., $RH_s$=RH), the evaporation fraction only relies on RH, regardless of surface water limitation or initial conditions.

## 2.3 MaxEnt with the extremum solution of the Monin-Obukhov similarity theory (MOST): a special case

Both MaxEnt and ETRHEQ utilize MOST and Businger–Dyer stability functions to describe the land–atmosphere system, but the MaxEnt model is based on a special formulation called the extremum solution of the Monin-Obukhov Similarity Theory (MOST). It is developed based on the hypothesis that: “Within the atmospheric surface layer in an environment for which the MOST applies, momentum flux would reach such values as to minimize heat flux and wind shear under stable conditions and to minimize heat flux and temperature gradient under unstable conditions."(Wang and Bras, 2010). Although the linkage between MaxEnt, ETRHEQ, and SFE in the steady state (as demonstrated above) does not depend on MOST's extremum solution, a question remains regarding the hydrometeorological interpretation of the extremum solution of MOST.

Recall in MOST, the temperature profile can be expressed as:

$$\frac{\kappa z}{\theta^*}\frac{\partial\theta}{\partial z} = \varphi_h(\frac{z}{L}) \tag{22}$$

where z is the height above the evaporation surface, θ is the potential temperature, θ* is the characteristic dynamical potential temperature, $\varphi_h(\frac{z}{L})$ is the stability function, and the L is the Obukhov length.

And the sensible heat is expressed as:

$$H = \rho c_p \overline{\omega'\theta'} \tag{23}$$

$$\overline{\omega'\theta'} = -K_h\frac{\partial\theta}{\partial z} = u^*\theta^* \tag{24}$$

where $\omega'$ and $\theta'$ are the perturbations of vertical velocity and potential temperature, respectively. $K_h$ is the eddy diffusivity for heat, and u* is the friction velocity. To distinguish the eddy diffusivity for heat as defined by the Monin-Obukhov Similarity Theory (MOST) from the MaxEnt model, the notation '$K_h$' is used instead of '$K_H$'.

Combining Eq. 22-24, the eddy diffusivity for heat based on MOST can be expressed as:

$$K_h = -\frac{\kappa u^* z}{\varphi_h(\frac{z}{L})} \tag{25}$$

Substituting $K_H$ from Eq. 6 into Eq. 25 from Wang and Bras (2009) leads to

$$\varphi_h(\frac{z}{L}) = -\frac{1}{C_1} \tag{26}$$

Combing Eq. 22, 23, 24 and 26, the temperature profile based on the extremum solution of MOST is thus described by the following:

$$\theta_s - \theta = \frac{H}{C_1 \kappa \rho c_p u^*} \ln\left(\frac{z}{z_0}\right) \quad (27)$$

By replacing the difference in surface and atmospheric potential temperature ($\theta_s$-$\theta$) with difference of surface and atmospheric temperature ($T_s$-T), and comparing Eq. 11 and 27, the parameterization of aerodynamic conductance in the MaxEnt model is obtained as:

$$g_a = \frac{C_1 \kappa u^*}{\ln\left(\frac{z}{z_0}\right)} \quad (28)$$

with the constant $C_1$ being defined in Wang and Bras (2009) for stable and unstable atmosphere condition, respectively.

Clearly, if $C_1$ is not considered, the inverse of Eq. 28 bears a resemblance to the classical aerodynamic resistance formula (e.g., FAO PM equation as presented in Eq. 29) (Allen et al., 1998) for neutral atmospheric conditions (i.e., $u^* = \frac{\kappa u}{\ln(\frac{z}{z_0})}$, where u is the mean wind speed at the measurement height z) (Stull, 1988), neglecting the displacement height (d) and the differences in roughness length on momentum, heat, and vapor exchange (i.e., $z_{om}=z_{oh}=z_0$):

$$g_a = \frac{\kappa^2 u}{\ln\left(\frac{z-d}{z_{om}}\right)\ln\left(\frac{z-d}{z_{oh}}\right)} \quad (29)$$

Currently, a common way to account for atmospheric stability is to multiply the aerodynamic conductance ($g_a$) with a correction factor, for example, in Merlin et al. (2016), the corrected aerodynamic conductance ($g_{ah}$) is expressed as:

$$g_{ah} = (1 + R_i)^{\eta} \cdot g_a \quad (30)$$

$$R_i = \frac{\beta_{thermal} \times g z_u (T_s - T_a)}{T_a u^2} \quad (31)$$

where $\beta_{thermal}$ is the thermal expansion coefficient, $\beta_{thermal}$ =5 following Choudhury et al. (1986) and Merlin et al. (2011); g is the gravitational constant, $T_s$ is the surface soil temperature; $T_a$ is the air temperature. In Eq. (30), the coefficient η is set to 0.75 in unstable conditions ($T_s > T_a$) and to 2 in stable conditions ($T_s < T_a$); u is the wind speed and $z_u$ is the height at which wind speed was measured.

Hence, the extremum solution of the MOST represents a simplified way to account for the atmospheric stability by assuming a constant correction factor ($C_1$) for stable and unstable atmosphere, respectively. As mentioned, the extremum solution is derived from the hypothesis concerning the equilibrium behavior of momentum fluxes and the resulting heat and water vapor fluxes, characterizing a unique atmospheric condition. Its connection with the maximum information entropy theory is unclear, which still requires further investigation (Wang and Bras, 2010).

More importantly, the linkage between MaxEnt with ETRHEQ and SFE in the steady state does not rely on the extremum solution of MOST, showing that predicting surface energy fluxes by minimizing D can be applied without the parameterization of extremum solutions of MOST. This leads to a more general expression of D, as:

$$D = \frac{2G^2}{I_s} + \frac{2H^2}{I_a} + \frac{LE^2}{I_e} \quad (32)$$

with $I_s = \sqrt{I_d^2 + \theta\, I_w^2}$, $I_a = \rho c_p \sqrt{g_a}$, and $I_e = \frac{\delta}{\gamma} RH_s I_a$.

The generalized formulation incorporating equations like Eq. 30 and 31 to correct $g_a$ for various atmospheric stability conditions may lead to improved performance, and this remains the subject of ongoing research.

## 3. The connection between the MaxEnt, ETRHEQ, and SFE in the non-steady state

The idealized box model of the atmospheric boundary layer proposed by McColl et al. (2019) was used to demonstrate the connection between the MaxEnt, ETRHEQ, and SFE in the non-steady state. The box and its governing equations for heat and moisture budget are presented in Figure 1. The rest of the parameters are described in McColl et al. (2019).

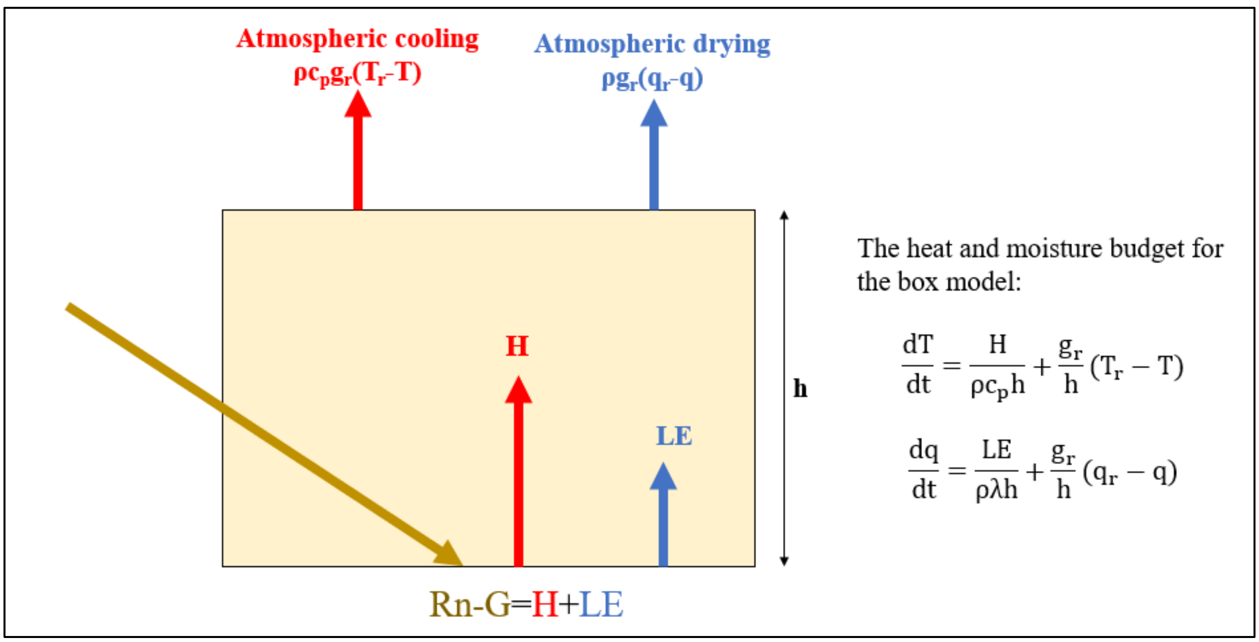


**Figure 1. The conceptualization of the idealized box model of the atmospheric boundary layer (ABL) and its the heat and moisture budgets. The figure was adapted from McColl et al. (2019). Rn is the net radiation, G is the ground heat flux, H is the sensible heat and LE is the latent heat. The box has depth h, potential temperature T, specific humidity q, air**

**density ρ, and specific heat of air $c_p$. The atmospheric cooling and drying conductance are denoted as $g_r$. $T_r$ is the atmospheric cooling relaxation temperature and $q_r$ is the atmospheric drying relaxation specific humidity.**

The box model converges to a steady state for a given set of initial conditions and parameters. Using the baseline parameters defined in McColl et al. (2019), the changes of LE, T, $T_s$, and RH with time up to 25 days are presented in Figure 2 (a-c). The simulation results obtained resembles those presented in McColl et al. (2019). The vertical differences of RH and the vertical variance of RH for each timestep are presented in Figure 2 (d-e). Clearly, the gradual decrease in dissipation accompanies the gradually increasing vertical difference of RH, and as they approach the steady state, their curves become flat. Based on the simulation results, the minimum dissipation does not correspond to the minimum vertical difference of RH and the minimum vertical variance of RH over the simulation period. This occurs as RH keeps rising even after reaching RH=$RH_s$. However, the vertical RH gradient typically diminishes towards zero, as explained in Kim et al. (2021). As this gradient of relative humidity vanishes, the system eventually attains a state known as "surface fluxes equilibrium." To incorporate SFE in the box model, $\frac{dT}{dt}$ and $\frac{dq}{dt}$ are forced to zero once the vertical component of Relative Humidity (RH) vanishes. The updated box model was run under identical initial conditions and parameters, with the outcomes displayed in Figure 3. The added constraint ensures that the model reaches SFE in its steady state.

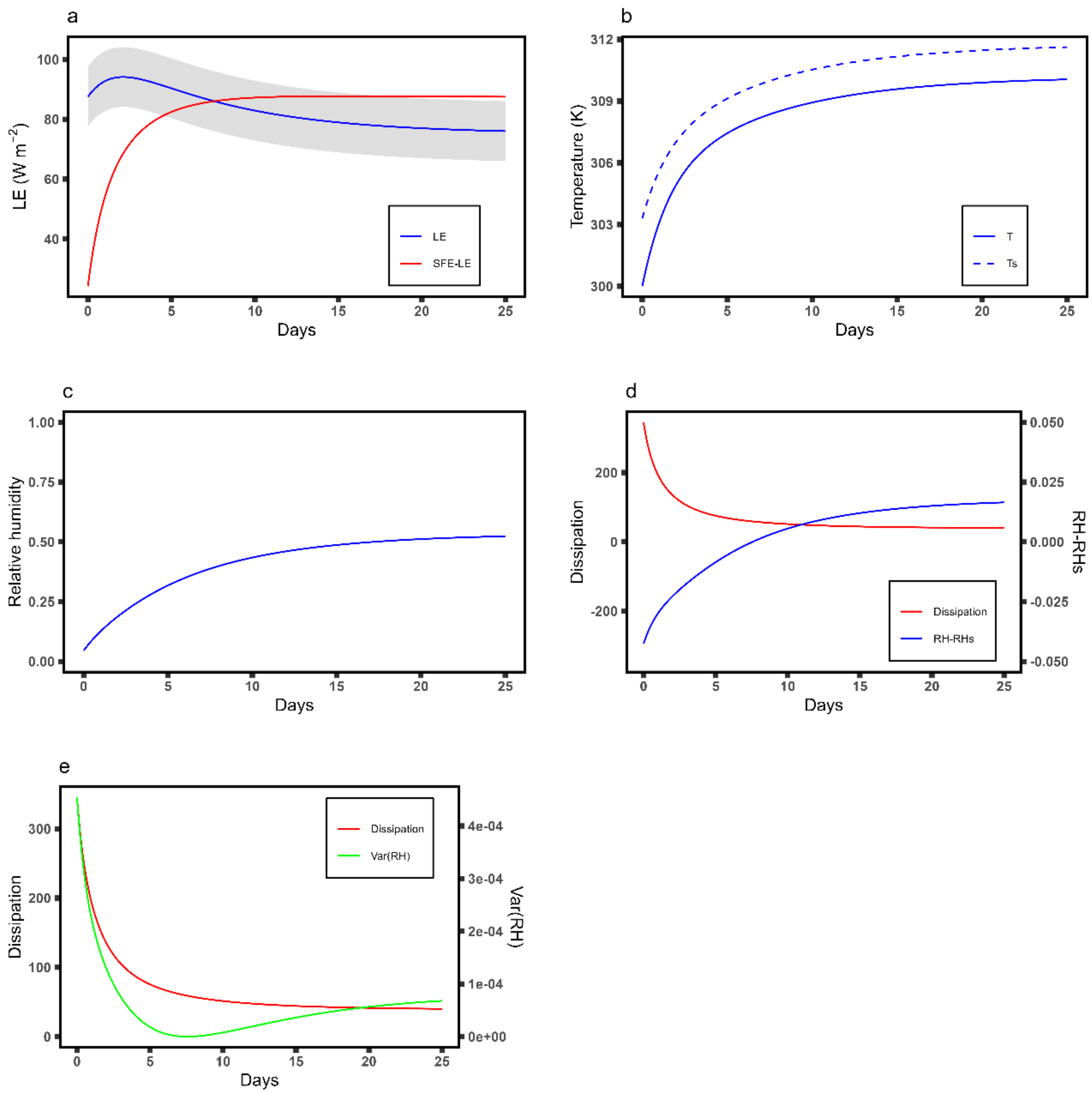


**Figure 2. Example behavior of the box model in the baseline case. The baseline values for each parameter were provided in McColl et al. (2019). (a) Traces of LE and the estimated LE using Eq. 1.The shaded region was plotted as ± 10 W m$^{-2}$ to represent the uncertainty following McColl et al. (2019). (b) Traces of surface temperature ($T_s$) and air potential temperature (T). (c) Traces of relative humidity RH within the box. (d) Traces of the vertical difference of RH (calculated as RH minus $RH_s$) and the dissipation (D) using Eq. 32. (e) Traces of the vertical variance of RH (denoted as Var(RH), and the dissipation (D)**

**using Eq. 32. The initial state of air potential temperature and specific humidity are 300 (K) and 0.001 (kg/kg), respectively.**

The RH budget of the updated box model is outlined in Equation B1 in McColl et al. (2019), where the sensitivity of the box model to various parameters was examined as well. Therefore, this paper will not delve into these details again to avoid redundancy. Briefly, the steady state and the time taken to reach it are influenced by several factors. These include energy forcings such as downwelling longwave and shortwave radiations, atmospheric cooling and drying conditions (i.e.,$T_r$ and $q_r$), the height of the ABL (i.e., h), the inverse sensitivity of the equilibrium ABL state to changes in surface fluxes (represented by $g_r/g_a$), and various surface conditions (such as surface conductance, surface albedo, ground heat flux conductivity, etc.) (McColl et al., 2019). The difference in the steady state between the two box models, as shown in Figures 2 and 3, usually occurs when $g_s$ is small and or $g_r/g_a$ is high, indicating that the state of ABL is predominantly influenced by the external atmosphere (McColl et al., 2019). Regardless of how these factors change, the dissipation (D) consistently decreases as the vertical variance of RH diminishes, until the system attains a steady state. This aligns with the mathematical analysis presented in the previous section.

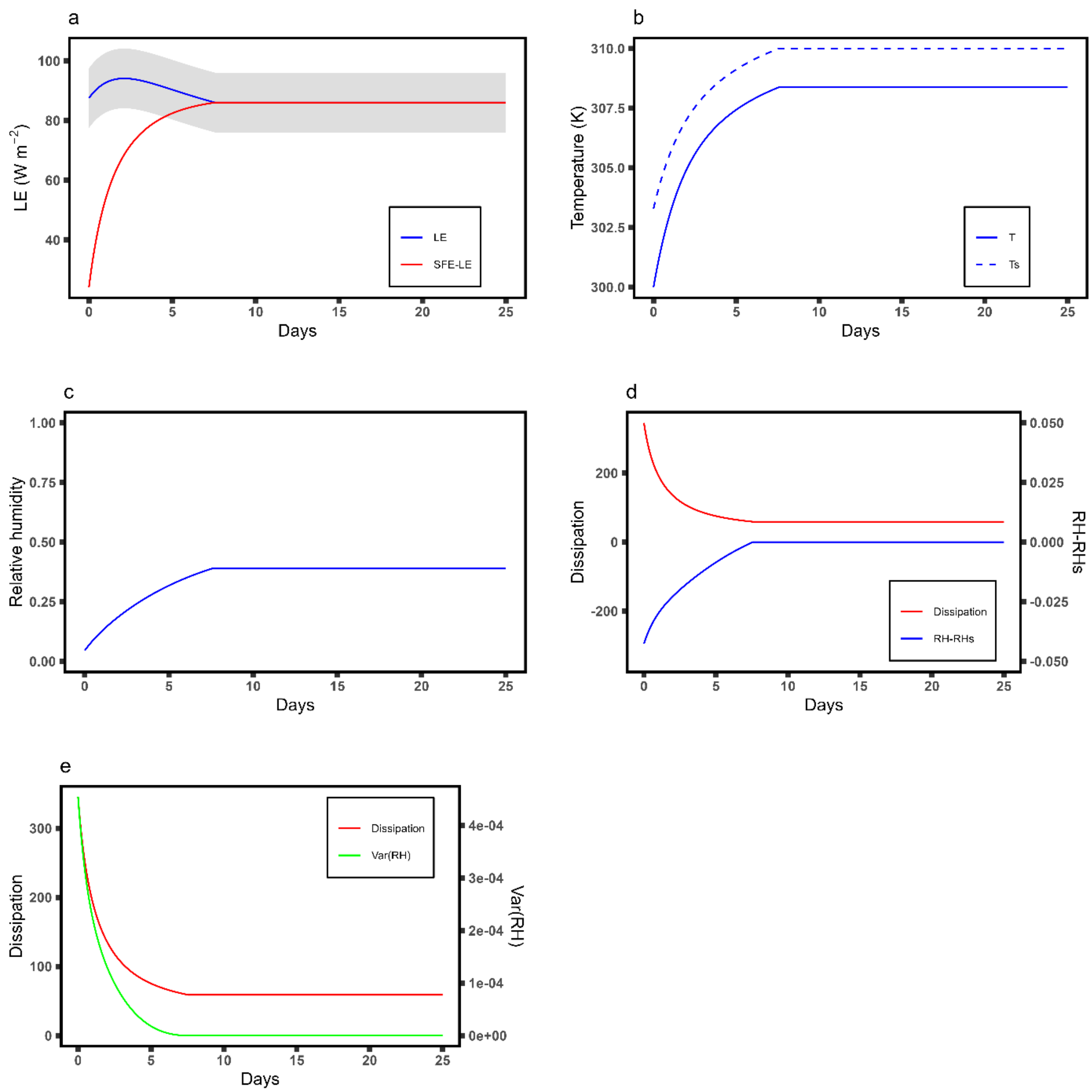


**Figure 3. Example behavior of the updated box model in the baseline case. The updated box model forced the model reaches SFE in its steady state. The baseline values for each parameter were provided in McColl et al. (2019). (a) Traces of LE and the estimated LE using Eq. 1.The shaded region was plotted as ± 10 W m$^{-2}$ to represent the uncertainty following McColl et al. (2019). (b) Traces of surface temperature (Ts) and air potential temperature (T). (c) Traces of relative humidity RH within the box. (d) Traces of the**

**vertical difference of RH (calculated as RH minus RHs) and the dissipation (D) using Eq. 32. (e) Traces of the vertical variance of RH (denoted as Var(RH), and the dissipation (D) using Eq. 32. The initial state of air potential temperature and specific humidity are 300 (K) and 0.001 (kg/kg), respectively.**

Recall that in ETRHEQ, optimal daily surface conductance minimizes the vertical variance of RH over a day. Therefore, the updated box model is employed to examine how the vertical variances of RH and D react to different values of $g_s$, while keeping all other parameters consistent with those specified in the baseline. Figure 4 illustrates that in conditions far from the steady state, a lower $g_s$ correlates to both lower Var(RH) and lower D. However, as the system nears steady state (as seen in the 4-6 day range in Figure 4b), a lower $g_s$ corresponds to a higher Var(RH). This is because a lower $g_s$ leads to a more gradual decrease in Var(RH) until it eventually reaches zero. In ETRHEQ, the optimal $g_s$ is calculated using weather data on a subdaily basis. Variations in the data at this finer scale suggest that the system in focus is typically far from steady state, because the Var(RH) in the real case is usually greater than 0.01 (e.g. Figure 2 in Salvucci and Gentine (2013)). Therefore, identifying the optimal surface conductance that minimizes Var(RH) from subdaily weather data in ETRHEQ is similar to minimizing dissipation, or in other words, maximizing the entropy production of the system. In this regard, ETRHEQ is akin to MaxEnt when the system is far from steady state.

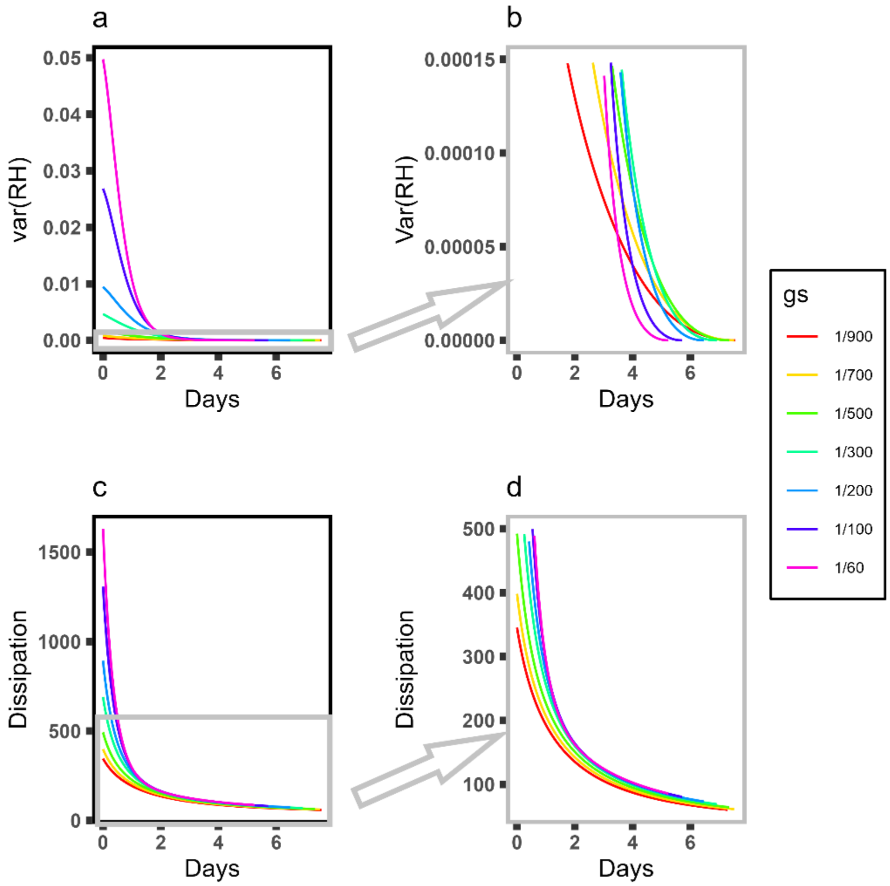


**Figure 4. Traces of the vertical variance of RH (panel a) and the dissipation (panel c) until the box reached the steady state. The simulation was run with the baseline parameters defined in McColl et al. (2019) and varying surface conductance ($g_s$). The initial state of air potential temperature and specific humidity are 300 (K) and 0.001 (kg/kg), respectively. The section highlighted in the gray square is enlarged in panels b and d, respectively.**

## 5. Model divergences, limitations, and implications

Despite having an equivalent physical foundation, MaxEnt and ETRHEQ diverge when it comes to their treatment of vegetation's role in evapotranspiration. Recall that in MaxEnt, the parameter 'z' represents the distance above the evaporation surface. For bare soil conditions, 'z' is the height above the land surface, whereas for vegetated surfaces, 'z' is the height above the vegetation canopy (Wang and Bras, 2011). Therefore, MaxEnt addresses vegetation transpiration by designating the leaf surfaces as the evaporation surface. As a result, the ground heat flux (G) in D is either omitted or considered as the heat flux within the canopy, and the surface temperature ($T_s$) and the specific surface humidity ($q_s$) is interpreted as the temperature and humidity at the leaf surface (Wang and Bras, 2011). In the case of heterogeneous vegetated ecosystems, MaxEnt calculates evapotranspiration by separately estimating evaporation for bare soil and transpiration for the vegetation. These estimates are then combined by taking into account the vegetation fractions of the site, which are derived from satellite imagery (Yang et al., 2022). In contrast, ETRHEQ sets the momentum roughness as 0.1 times the vegetation height, and it estimates the roughness heights for heat and water vapor using the $kB^{-1}$ method, which links the momentum roughness to the roughness heights for heat and water vapor (Rigden and Salvucci, 2015; Salvucci and Gentine, 2013). For heterogeneous vegetated sites, Rigden and Salvucci (2015) used different $kB^{-1}$ values to accommodate these differences and combined the results via a weighted average. Hence, the accuracy of MaxEnt in predicting evapotranspiration on vegetated surfaces relies on the precision of leaf surface temperature and specific humidity measurements (or estimation), while that of ETRHEQ depends on the validity of the assumptions regarding the roughness heights for momentum, heat, and vapor. Furthermore, at the steady state, where the land surface $RH_s$ matches the atmospheric RH at the reference height, it also implies that the leaf surface relative humidity ($RH_{leaf}$) is the same with both $RH_s$ and RH, leading to convergence of both MaxEnt and ETRHEQ into the SFE state.

As previously noted, while the SFE model and the ETRHEQ model demonstrate good performance in inland continental regions, they proved less suitable for locations characterized by substantial horizontal moisture advection, such as coastal regions, and for sites with extremely arid or humid soil conditions (Chen et al., 2021; Raghav and Kumar, 2021). In contrast, the MaxEnt model demonstrated superior performance on densely vegetated surfaces, such as tropical rainforests and well-watered wetland areas; however, it displayed more noticeable disparities when applied to areas with shorter vegetation, like shrublands, primarily because of the approximation of surface temperature and specific humidity using air temperature and humidity (Yang et al., 2022). While these models exhibit varying performance in diverse ecosystems, their shared physical foundation implies that they have common limitations, such as the omission of horizontal moisture advection. The discrepancies in their performance primarily arise from the accuracy of the measured variables utilized as inputs for the models and the methodologies employed to address surface heterogeneity.

The intrinsic connection between the vertical RH profile and the dissipation function, rooted in Shannon information entropy, establishes the foundational principle for integrating MaxEnt, ETRHEQ, and SFE within a cohesive hydrometeorological framework. Particularly, Eq. 32 aligns with ETRHEQ when considering the energy balance constraint, eliminating the need for subdaily meteorological variables as inputs, which suggests a broader range of potential applications compared to ETRHEQ. More importantly, the empirical success of MaxEnt, ETRHEQ and SFE suggests that turbulence fluxes within the atmospheric boundary layer adhere to the principles of information entropy. The manner in which dissipation is formulated (Eq. 32) within information entropy theory differs from classical thermodynamic entropy formulations, such as those proposed by Kleidon (2009) or Brunsell et al. (2011). How to properly calculate dissipation and entropy production for energy fluxes at different temporal and spatial scales presents an intriguing avenue for future research.

## 6. Conclusion

This paper presents a pure theorical analysis to unifying the three most widely used parsimonious models, MaxEnt, ETRHEQ and SFE, within a single hydrometeorological framework. Analysis here demonstrates that determining the optimal surface conductance in ETRHEQ that minimizes the vertical variance of RH is equivalent to minimizing the dissipation function of energy fluxes in MaxEnt. The empirical success of both MaxEnt and ETRHEQ lies in the fact that the far-from-equilibrium ecosystems progress toward a steady state by minimizing dissipation. This tendency is manifested through the vertical variance of RH. The connection between MaxEnt, ETRHEQ, and SFE is independent of MOST's extremum solution which can be viewed as equivalent to introducing a constant correction factor to account for atmospheric stability.

While MaxEnt and ETRHEQ share a common physical foundation, they diverge in their approaches to modeling evapotranspiration, particularly in how they address the roles of vegetation and land surface heterogeneity. More importantly, the unified hydrometeorological framework suggests that turbulence fluxes within the atmospheric boundary layer adhere to the principles of maximum information entropy production theory. The manner in which dissipation (and associated entropy production) is formulated based on information entropy theory differs from classical thermodynamic entropy production formulations. Exploring the accurate calculation of dissipation and entropy production for energy fluxes across various temporal and spatial scales offers an enticing prospect for future research.

## Appendix A Derivation of Eq. 7

The vertical profile of RH can be determined through the chain rule as:

$$\frac{\partial RH}{\partial z} = \frac{\partial RH}{\partial q^*(T)}\frac{\partial q^*(T)}{\partial T}\frac{\partial T}{\partial z} + \frac{\partial RH}{\partial q}\frac{\partial q}{\partial z} = \frac{-q}{\left(q^*(T)\right)^2}\frac{\partial q^*(T)}{\partial T}\frac{\partial T}{\partial z} + \frac{\partial RH}{\partial q}\frac{\partial q}{\partial z} = \frac{-RH}{q^*(T)}\frac{\partial q^*(T)}{\partial T}\frac{\partial T}{\partial z} + \frac{\partial RH}{\partial q}\frac{\partial q}{\partial z} = \frac{1}{q^*(T)}\left(-\delta \cdot RH \cdot \frac{\partial T}{\partial z} + \frac{\partial q}{\partial z}\right) \tag{A1}$$

where $RH = \frac{q}{q^*(T)}$, $q^*(T)$ is the saturated specific humidity at temperature T, and $\delta = \frac{\partial q^*(T)}{\partial T}$.

## Appendix B Derivation of Eq. 17

Under the constraint of energy closure, substituting Eq. 10 into the energy balance, the sensible H can be expressed as:

$$H = Rn - G - \frac{RH_s\delta(Rn - G)}{RH_s\delta + \gamma} - \frac{\rho c_p q^*\left(T_s\right)\left(RH_s - RH\right)g_a}{RH_s\delta + \gamma} \tag{B1}$$

Substituting Eq. B1, 10, 11, 15, 16 into Eq.2, the dissipation can be rearranged as:

$$D = \frac{2\left(\left(q^*\left(T_s\right)^2 c_p^2 g_a^2\left(-RH_s + RH\right)^2(\sigma + 1)\rho^2 - 2q^*\left(T_s\right)c_p g_a\left(-RH_s + RH\right)\left(-RH_s\delta + \gamma\sigma\right)(-Rn + G)\rho + (-Rn + G)^2\left(RH_s^2\delta^2 + \gamma^2\sigma\right)\right)I_s + G^2\left(RH_s\delta + \gamma\right)^2\rho c_p\sqrt{g_a}\sigma\right)}{\sqrt{g_a}I_s\left(RH_s\delta + \gamma\right)^2\rho c_p\sigma}$$

$$\xrightarrow{\textit{Rearrange}}$$

$$D = \frac{2q^*\left(T_s\right)^2 c_p g_a^2(\sigma + 1)\rho}{\sqrt{g_a}\left(RH_s\delta + \gamma\right)^2\sigma}\left(-RH_s + RH\right)^2 - \frac{4q^*\left(T_s\right)c_p g_a\left(-RH_s\delta + \gamma\sigma\right)(-Rn + G)\rho}{\sqrt{g_a}\left(RH_s\delta + \gamma\right)^2\rho c_p\sigma}\left(-RH_s + RH\right) + \frac{2I_s(-Rn + G)^2\left(RH_s^2\delta^2 + \gamma^2\sigma\right) + 2G^2\left(RH_s\delta + \gamma\right)^2\rho c_p\sqrt{g_a}\sigma}{\sqrt{g_a}I_s\left(RH_s\delta + \gamma\right)^2\rho c_p\sigma} \tag{B2}$$

## Open research

Data were not used, nor created for this research. Software (other than for typesetting) was not used for this research. The replication of Figures 2, 3, and 4 in the paper is facilitated by the R programming codes provided by Wang, Y. (2023). These codes, titled "R programming codes for generating figures in Paper # 2023WR036910," are accessible on Zenodo at https://doi.org/10.5281/zenodo.10403193.

**Acknowledgement**

The authors wish to express their gratitude to the three anonymous reviewers for their comprehensive and insightful feedback on our prior work, which served as the inspiration for this study. We also extend our thanks to Jiseok Lee for providing feedback on the mathematical proofs. We would also like to acknowledge ChatGPT in enhancing the clarity and coherence of our manuscript.

**Funding information**

We would like to thank the Mountain Water Futures project of the Global Water Futures programme (Canada First Research Excellence Fund), Alberta Innovates – Energy and Environment Solutions (Grant #'s: AIES-2335, 2335 20007947; Rooney, Petrone), and the Canadian Natural Science and Engineering Research Council (NSERC) Discovery (RGPN-04182-2017; Petrone) and CREATE (463960-2015; Petrone) grants programs for the financial support.

**References:**

Allen, R.G., Pereira, L.S., Raes, D. and Smith, M., 1998. Crop evapotranspiration-Guidelines for computing crop water requirements-FAO Irrigation and drainage paper 56. FAO, Rome, 300(9): D05109.

Brunsell, N.A., Schymanski, S.J. and Kleidon, A., 2011. Quantifying the thermodynamic entropy budget of the land surface: is this useful? Earth System Dynamics, 2(1): 87-103.

Businger, J.A., Wyngaard, J.C., Izumi, Y. and Bradley, E.F., 1971. Flux-profile relationships in the atmospheric surface layer. Journal of the atmospheric Sciences, 28(2): 181-189.

Chen, S., McColl, K.A., Berg, A. and Huang, Y., 2021. Surface Flux Equilibrium Estimates of Evapotranspiration at Large Spatial Scales. Journal of Hydrometeorology, 22(4): 765-779.

Choudhury, B.J., Reginato, R.J. and Idso, S.B., 1986. An analysis of infrared temperature observations over wheat and calculation of latent heat flux. Agricultural and Forest Meteorology, 37(1): 75-88.

Dewar, R.C., 2005. Maximum entropy production and the fluctuation theorem. Journal of Physics A: Mathematical and General, 38(21): L371.

Dickinson, R.E., 1983. Land surface processes and climate—Surface albedos and energy balance, Advances in geophysics. Elsevier, pp. 305-353.

Duveiller, G., Hooker, J. and Cescatti, A., 2018. The mark of vegetation change on Earth's surface energy balance. Nat Commun, 9(1): 679.

Edlefsen, N. and Anderson, A., 1943. Thermodynamics of soil moisture. Hilgardia, 15(2): 31-298.

Jaynes, E.T., 1957. Information theory and statistical mechanics. Physical review, 106(4): 620.

Kim, Y., Garcia, M., Black, T.A. and Johnson, M.S., 2023. Assessing the complementary role of Surface Flux Equilibrium (SFE) theory and Maximum Entropy Production (MEP) principle in the estimation of actual evapotranspiration. Journal of Advances in Modeling Earth Systems, 15(7): e2022MS003224.

Kim, Y. et al., 2021. Relative humidity gradients as a key constraint on terrestrial water and energy fluxes. Hydrology and Earth System Sciences, 25(9): 5175-5191.

Kleidon, A., 2009. Nonequilibrium thermodynamics and maximum entropy production in the Earth system: applications and implications. Naturwissenschaften, 96(6): 1-25.

Lent, C.S., 2019. Information and entropy in physical systems. Energy Limits in Computation: A Review of Landauer's Principle, Theory and Experiments: 1-63.

McColl, K.A., Salvucci, G.D. and Gentine, P., 2019. Surface flux equilibrium theory explains an empirical estimate of water-limited daily evapotranspiration. Journal of Advances in Modeling Earth Systems, 11(7): 2036-2049.

Merlin, O. et al., 2011. An Analytical Model of Evaporation Efficiency for Unsaturated Soil Surfaces with an Arbitrary Thickness. Journal of Applied Meteorology and Climatology, 50(2): 457-471.

Merlin, O. et al., 2016. Modeling soil evaporation efficiency in a range of soil and atmospheric conditions using a meta-analysis approach. Water Resources Research, 52(5): 3663-3684.

Monteith, J.L., 1965. Evaporation and environment, Symposia of the society for experimental biology. Cambridge University Press (CUP) Cambridge, pp. 205-234.

Priestley, C.H.B. and Taylor, R.J., 1972. On the Assessment of Surface Heat Flux and Evaporation Using Large-Scale Parameters. Monthly Weather Review, 100(2): 81-92.

Prigogine, I. and Lefever, R., 1973. Theory of Dissipative Structures. In: H. Haken (Editor), Synergetics: Cooperative Phenomena in Multi-Component Systems. Vieweg+Teubner Verlag, Wiesbaden, pp. 124-135.

Raghav, P. and Kumar, M., 2021. Retrieving gap-free daily root zone soil moisture using surface flux equilibrium theory. Environmental Research Letters, 16(10): 104007.

Rigden, A.J. and Salvucci, G.D., 2015. Evapotranspiration based on equilibrated relative humidity (ETRHEQ): Evaluation over the continental US. Water Resources Research, 51(4): 2951-2973.

Salvucci, G.D. and Gentine, P., 2013. Emergent relation between surface vapor conductance and relative humidity profiles yields evaporation rates from weather data. Proceedings of the National Academy of Sciences, 110(16): 6287-6291.

Schneider, E.D. and Kay, J.J., 1994. Life as a manifestation of the second law of thermodynamics. Mathematical and computer modelling, 19(6-8): 25-48.

Stull, R.B., 1988. Boundary Conditions and Surface Forcings. In: R.B. Stull (Editor), An Introduction to Boundary Layer Meteorology. Springer Netherlands, Dordrecht, pp. 251-294.

Wang, J. and Bras, R.L., 2009. A model of surface heat fluxes based on the theory of maximum entropy production. Water Resources Research, 45(11).

Wang, J. and Bras, R.L., 2010. An Extremum Solution of the Monin–Obukhov Similarity Equations. Journal of the Atmospheric Sciences, 67(2): 485-499.

Wang, J. and Bras, R.L., 2011. A model of evapotranspiration based on the theory of maximum entropy production. Water Resources Research, 47(3).

Yang, Y., Sun, H., Zhu, M., Wang, J. and Zhang, W., 2022. An R package of maximum entropy production model to estimate 41 years of global evapotranspiration. Journal of Hydrology, 614: 128639.

Wang, Y. (2023). R programming codes for generating figures in Paper # 2023WR036910. Zenodo. https://doi.org/10.5281/zenodo.10403193. [Computational Notebook].